



Building shadow detection based on multi-thresholding segmentation

Ali J. Ghandour¹ · Abdelkarim A. Jezzini²

Received: 19 April 2018 / Revised: 3 September 2018 / Accepted: 5 September 2018
© Springer-Verlag London Ltd., part of Springer Nature 2018

Abstract

The human eye can easily identify shadows of illuminated objects. However, automatically detecting such shadows with the use of computer tools is a challenging research problem. In this paper, an approach toward successful building shadow detection based on multi-threshold image segmentation technique is introduced and analyzed. Accuracy assessment and computing time analyses conducted over seven study areas from two reference datasets show the high performance of our proposed approach in detecting real shadows with a 93.75% accuracy.

Keywords Building extraction · Remote sensing · Shadow detection · Hypothesis and validation · Object identification

1 Introduction

Shadow regions are the part of the image not directly illuminated by a light source due to the presence of a body intercepting the light. Presence of shadows in an image can reveal information about the objects' shape and orientation [1].

Generally, shadows can be divided into two major classes: (i) self-shadow and (ii) cast shadow. A cast shadow is the area projected by an object exposed to a direct light source. Most of the shadow detection methods focus on detecting cast shadows since they are correlated with the objects' geometric shape in the targeted image.

The presence of cast shadows in aerial images may cause objects' shape distortion and loss of feature information. Due to this reason, the topic of shadow detection and removal is given significant attention and consideration in the computer vision domain, covering many specific applications such as object detection [2], building elevation detection, [3] and building damage detection [4].

In this work, we will focus on the automatic detection of buildings' shadows in aerial images. The contribution of this manuscript is twofold: (i) We introduce a robust approach for accurate building shadow detection based on multi-thresholding image processing technique that we refer to as shadow detection multi-thresholding segmentation (*SMS*). (ii) An accuracy assessment, computing time analysis and space complexity are conducted over several study areas from two reference datasets showing the performance of the suggested method in terms of accuracy, time and space complexity.

The rest of this paper is divided as follows: Sect. 2 presents a review of published work on shadow detection approaches. Section 3 introduces our proposed shadow detection algorithm based on multi-thresholding segmentation. Section 4 presents the proposed algorithm benchmarking results with execution time and storage analysis. Section 5 presents the conclusion.

2 Literature review

A significant amount of research has been conducted in the literature focusing on the detection of shadows. Shadow detection usually has various purposes such as estimation of objects' shape, image enhancement and pattern or object recognition. Shadow detection methods can be classified according to the study performed in [5] into two main classes: (i) model based and (ii) feature based [6–8]. In this manuscript, we will focus on feature-based techniques.

Several subtypes of feature-based shadow detection methods exist in the literature [7]. For the scope of this manuscript,

✉ Ali J. Ghandour
aghandour@cnrs.edu.lb
Abdelkarim A. Jezzini
abdelkarim.j@gmail.com

¹ National Council for Scientific Research, CNRS, 59, Zahia Salmane Street, Jnah, P.O. Box 11-8281, Beirut, Lebanon

² Department of Computer and Communication Engineering, Islamic University of Lebanon, P.O. Box 30014, Beirut, Lebanon

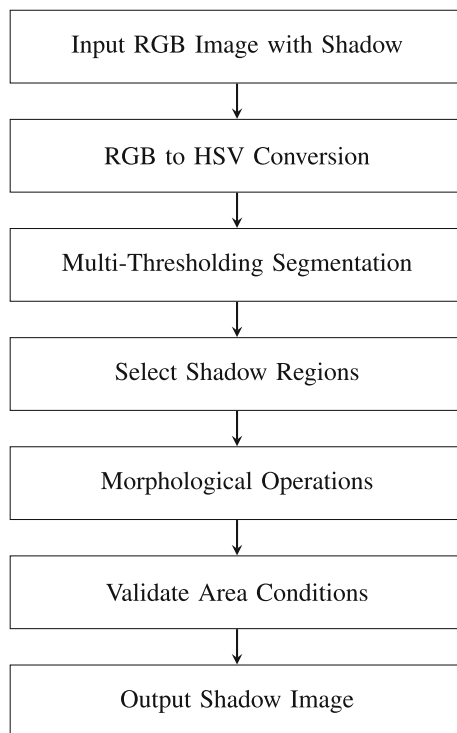


Fig. 1 Block diagram of *SMS* algorithm

we will focus only on the threshold-based shadow detection subtype of feature-based shadow detection algorithms. Threshold-based methods depend on the shadow features. A simple thresholding of value component in the *HSV* color space could be very promising as shown in [9,10].

In [11], Polodorio et al. proposed a threshold-based algorithm for aerial image shadow detection. They used the $(I-S)$ difference of the components of the *HSI* color space. Their approach relies on the hypothesis that *I* values decrease and *S* values increase with shadow. Hence, $(I-S)$ difference should be low for shadow regions and high for non-shadow regions.

Algorithm 1: Pseudo-code of *SMS* algorithm.

Input : RGB image

1 Pre-Processing:

- 2 RGB to HSV conversion
- 3 Luminance band extraction

4 Multi-thresholding Segmentation:

- 5 Luminance band quantization based on thresholds number *M*

6 Shadows Selection and Validation :

- 7 First class C_0 extraction
- 8 Erosion operation application based on structuring elements (*SE*)
- 9 Average shadow area *SA* computation
- 10 Shadow area validation

Output: Binary image with labeled shadows

The author of [6] introduced the Normalized Saturation Value Difference Index (*NSVDI*) threshold-based detection

algorithm for aerial images. It is shown in [6] that an improvement could be achieved in the performance of the previous $(I-S)$ difference threshold approach [11].

Zhang and Wenzhuo [12] proposed a new shadow detection method based on shadow features that they used in the segmentation process according to the Convexity Mode *CM*. After this process, histogram thresholding was applied and a shadow object candidate set was obtained by comparing the threshold and grayscale average of each object in the candidate set. Then, they eliminated false shadows such as vegetation areas according to the spatial information of the image. Finally, non-shadow candidates were ruled out to obtain the final results.

Zhang et al. [13] presented an automatic shadow detection algorithm by applying a bimodal histogram splitting method. Shadow detection results can exhibit both umbra and penumbra areas to increase the accuracy of the result.

Khan [14] presented a new methodology to automatically detect shadows in real-world study areas showcasing the most relevant features in a supervised manner by the use of multiple convolutional deep neural networks (*ConvNets*). The proposed framework examines features at the super-pixel level and along the object boundaries. The proposed framework consistently performed better than the state-of-the-art frameworks on all major shadow databases collected under a variety of conditions.

Huihui Song [15] proposed a novel shadow detection algorithm based on morphological filtering. An initial shadow mask was generated by the thresholding method, and then, the false shadow regions were removed by morphological filtering. Experimental results on QuickBird and WorldView-2 satellite images have shown that the proposed shadow detection technique can generate accurate shadow masks with great quality percentages.

Tsai [16] proposed a method that depends on the *HSI* color space and is based on the $(He+I)/(Ie+I)$ ratio threshold, where *He* is defined as Hue equivalent and *Ie* is defined as intensity equivalent components. *He* is selected as the *H* component in *HSI*, *HSV* and *HCV* color spaces. *Ie* is selected as the *I* component in the *HSI* color space, and as *V* in the *HSV* and *HCV* color spaces. The threshold was selected using the Otsu [17] method along with mentioning that a trade-off exists between the automation of the detection process and the accuracy of the shadow detection [16].

In addition, a simple threshold for the gray value of the image could be a choice since the best known feature of a shadow is the decreasing intensity [9,10]. The intensity equivalent component of any color space as defined in [16] could be selected as the gray value.

Shadow detection based on adaptive thresholding was employed and implemented by authors in [18]. They experimentally showed that this method is more effective than the existing fixed threshold shadow detectors in increasing set-

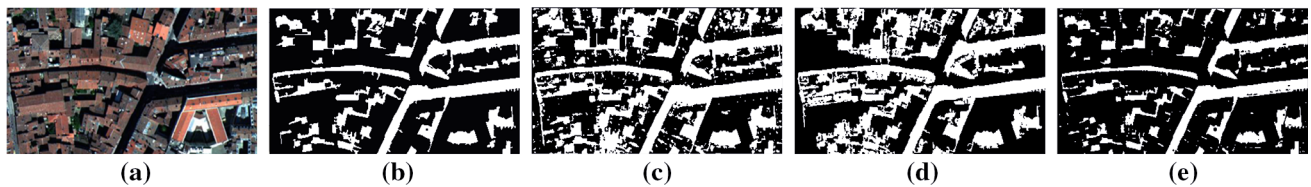


Fig. 2 a–e Show the original image and the output of applying SMS, M1, M2 and M3, on Urban Canyon Study Area, respectively

Table 1 Accuracy assessment of *SMS* and the three benchmarked algorithms on the Urban Canyon Study Area

Method	PA		UA		OA	F_Score
	P_s	P_n	U_s	U_n		
SMS	99.6	99.8	99.6	99.8	99.7	99.6
M1	96.3	97.8	95.0	98.4	97.3	95.6
M2	95.3	98.4	96.2	98.0	97.5	95.8
M3	98.1	98.2	95.9	99.2	98.2	97.0

Table 2 Accuracy assessment of *SMS* and the three benchmarked algorithms on St. Sermin Basilica Study Area

Method	PA		UA		OA	F_Score
	P_s	P_n	U_s	U_n		
SMS	97.2	98.6	96.7	98.1	97.8	96.4
M1	75.6	84.4	49.2	86.2	82.2	59.6
M2	91.5	98.4	92.9	98.1	97.2	92.2
M3	96.7	98.9	95.1	99.3	98.5	95.9

tlement classification accuracy. Shadow masking process is carried out based on the same and across date settlement accuracies. Finally, the statistical study applied showed that the shadow masking hypothesis is correct with a high accuracy performance.

More approaches that include various shadow features, based on input image properties, and also on the accuracy and simplicity necessary for the performance, might be found in [19].

3 Shadow detection multi-thresholding segmentation

In this paper, we propose an approach that depends mainly on a multi-thresholding technique. We refer to this approach as the shadow detection multi-thresholding segmentation (*SMS*). This method relies mainly on multi-level image thresholding to detect buildings' shadows.

As shown in the block diagram in Fig. 1, first, the input image is converted to the *HSV* color space followed by luminance band extraction. Thereafter, we apply the multi-thresholding technique on the luminance band which consists

of the defining threshold number. This is followed by luminance band quantization which tends to map each pixel luminance value to its closer threshold value. Then, we apply morphological operations in order to eliminate non-shadow regions. Finally, we use the area condition hypothesis to validate each shadow candidate object. Shadows of different objects such as trees or cars may be detected, and thus, the shadow area criteria are necessary to validate shadows related to buildings only. The pseudo-code for the *SMS* algorithm is shown in Algorithm 1.

Please note that after extracting the luminance band from the *HSV* color space by eliminating the hue and saturation information, the color information of all pixels within the converted image is represented by a value that measures pixels' closeness to black and white colors. This is referred to as pixel luminance.

3.1 Multi-thresholding formulation

The goal of image segmentation is to cluster pixels into salient image regions, i.e., regions corresponding to individual surfaces, objects or natural parts of objects. A seg-

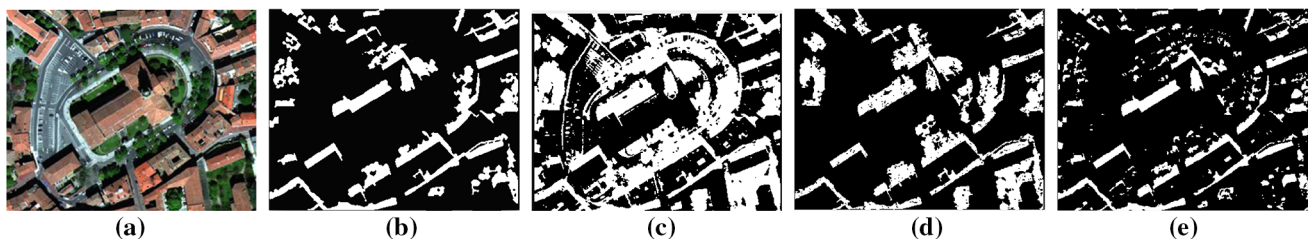


Fig. 3 a–e Show the original image and the output of applying SMS, M1, M2 and M3, on St. Sermin Basilica Study Area, respectively

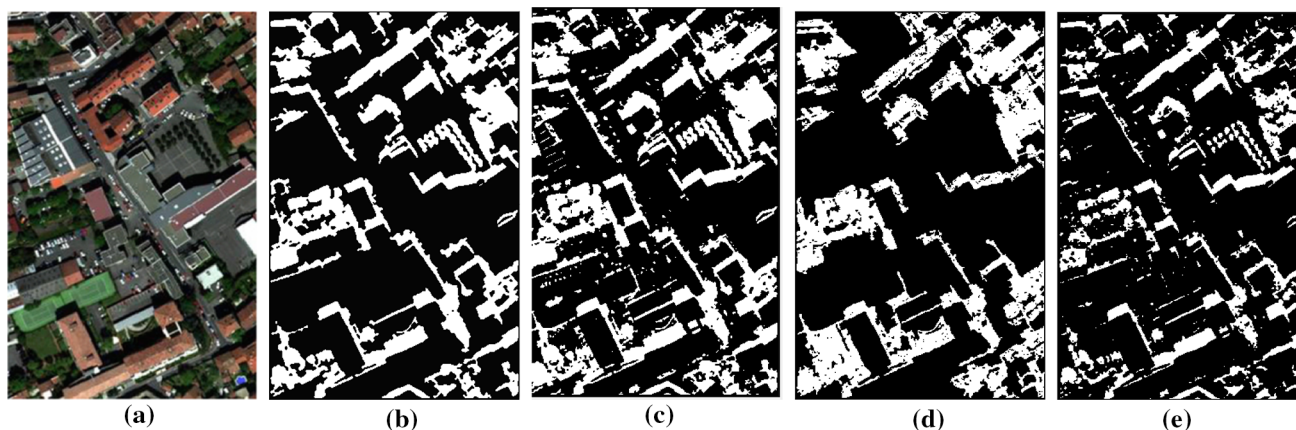


Fig. 4 a–e Show the original image and the resultant output of applying SMS, M1, M2 and M3, on Suburban Study Area, respectively

Table 3 Accuracy assessment of *SMS* and the three benchmarked algorithms on Toulouse Suburban Study Area

Method	PA		UA		OA	F_Score
	P_s	P_n	U_s	U_n		
SMS	92.4	97.8	94.6	96.6	95.1	93.4
M1	80.5	98.3	92.5	95.1	94.6	86.1
M2	84.8	97.2	88.6	96.1	94.6	86.7
M3	88.1	97.1	88.7	96.9	95.2	88.4

Table 4 Accuracy assessment of *SMS* and the three benchmarked algorithms on Garonne River Study Area

Method	PA		UA		OA	F_Score
	P_s	P_n	U_s	U_n		
SMS	99.8	99.1	90.9	99.9	98.4	95.1
M1	85.1	85.6	54.2	96.6	85.5	66.2
M2	86.0	85.3	53.9	96.8	85.4	66.3
M3	77.3	99.4	96.2	95.6	95.7	85.7

mentation could be used for object recognition, occlusion boundary, image compression and image editing.

There are several image segmentation techniques such as *k-means* clustering, *k-nn* segmentation and *maximum likelihood*. All these methods need more than one step in order to get the final segmented image along with the incurred implementation complexity. In our approach, we use the multi-thresholding technique based on the Otsu method. An optimal threshold is selected by the discriminant criterion to maximize the separability of the resultant classes in luminance levels by utilizing only the zeroth- and the first-order cumulative moments of the luminance band histogram. The use of multi-thresholding as a segmentation technique is more efficient with moderate implementation complexity and single-stage iteration.

Let the pixels of a given picture be represented in L luminance levels $[1, 2, \dots, L]$. The number of pixels at level i is denoted by n_i and the total number of pixels by $N = n_1 + n_2 + \dots + n_L$. In order to simplify the discussion, the luminance band histogram is normalized and regarded as a probability distribution according to [20]:

$$P_i = \frac{n_i}{N}, \quad \text{where } P_i \geq 0 \quad \text{and} \quad \sum_{i=1}^L P_i = 1 \quad (1)$$

Suppose we dichotomize the pixels into two classes C_0 and C_1 by using a threshold at level K . C_0 denotes pixels with levels $[1, K]$, and C_1 denotes pixels with levels $[K + 1, L]$. Then, the probabilities of class occurrence ω_0 and ω_1 and the class mean levels μ_0 and μ_1 , respectively, according to [20], are given by the following:

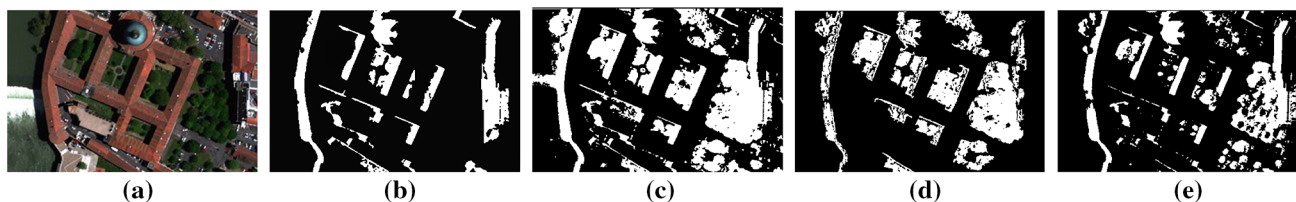


Fig. 5 a–e Show the original image and the output of applying SMS, M1, M2 and M3, on Garonne River Study Area, respectively

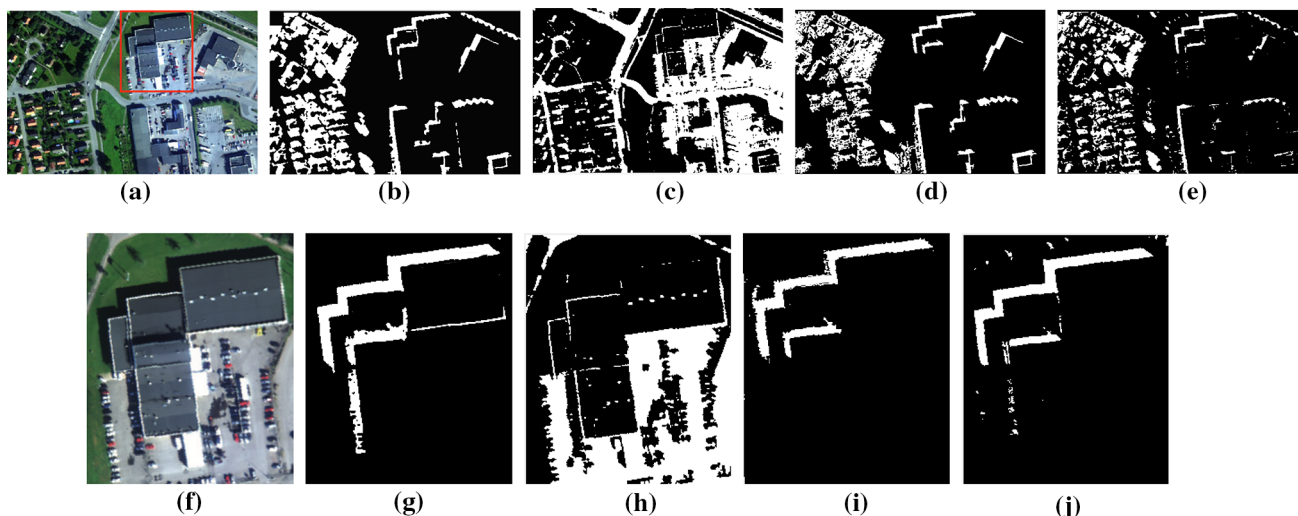


Fig. 6 a–e Show the original image and the output of applying SMS, M1, M2 and M3, on Norrköping Industrial Study Area, respectively. f–j Show a closeup of highlighted region (red frame) and the output of applying SMS, M1, M2 and M3, on it, respectively (color figure online)

Table 5 Accuracy assessment of SMS and the three benchmarked algorithms on Norrköping Industrial Study Area

Method	PA		UA		OA	F_Score
	P_s	P_n	U_s	U_n		
SMS	93.7	97.4	94.2	95.8	96.3	93.9
M1	92.6	84.4	54.5	98.3	85.8	68.6
M2	66.7	96.5	79.5	93.5	91.5	72.5
M3	94.1	98.3	91.8	98.8	97.6	92.9

Table 6 Time and space complexities of benchmarked algorithms

Benchmarked algorithm	SMS	M1	M2	M3
Executorial time	0.4925	1.7197	1.3690	1.2109
Space complexity	$O(n^2)$	$O(n)$	$O(n)$	$O(n^2)$

$$\omega_0 = P_r(C_0) = \sum_{i=1}^K P_i = \omega(K) \tag{2}$$

$$\omega_1 = P_r(C_1) = \sum_{i=K+1}^L P_i = 1 - \omega(K) \tag{3}$$

$$\mu_0 = \sum_{i=1}^K i P_r(i|C_0) = \sum_{i=1}^K \frac{i P_i}{\omega_0} = \frac{\mu(K)}{\omega(K)} \tag{4}$$

$$\mu_1 = \sum_{i=K+1}^L i P_r(i|C_1) = \sum_{i=K+1}^L \frac{i P_i}{\omega_1} = \frac{\mu_T - \mu(K)}{1 - \omega(K)} \tag{5}$$

where $\omega(K)$ and $\mu(K)$ are the zeroth- and the first-order cumulative moments of the histogram up to the K th level, respectively, and μ_T is the total mean level of the original

picture. Following this, class variances are defined as:

$$\sigma_0^2 = \sum_{i=1}^K (i - \mu_0)^2 P_r(i|C_0) = \sum_{i=1}^K (i - \mu_0)^2 \frac{P_i}{\omega_0} \tag{6}$$

$$\sigma_1^2 = \sum_{i=K+1}^L (i - \mu_1)^2 P_r(i|C_1) = \sum_{i=1}^{K+1} (i - \mu_1)^2 \frac{P_i}{\omega_1} \tag{7}$$

Now, to evaluate the threshold goodness (at any level K), we use the total variance of levels η proposed in [21] and defined in Eq. 8. η is considered as the evaluation metric, used to measure class separability at level K . The main challenge that exists in the optimization problem is to search for a threshold K that maximizes η .

$$\eta = \frac{\sigma_B^2}{\sigma_T^2} \tag{8}$$

where

$$\sigma_B^2 = \omega_0(\mu_0 - \mu_T)^2 + \omega_1(\mu_1 - \mu_T)^2 \tag{9}$$

and

$$\sigma_T^2 = \sum_{i=1}^L (i - \mu_T)^2 P_i \tag{10}$$

The optimal threshold that maximizes η or equivalently maximizes σ_B^2 (since σ_T^2 is independent of K) is defined as K^* .

$$\sigma_B^2(K^*) = \max(\sigma_B^2(K)) \tag{11}$$

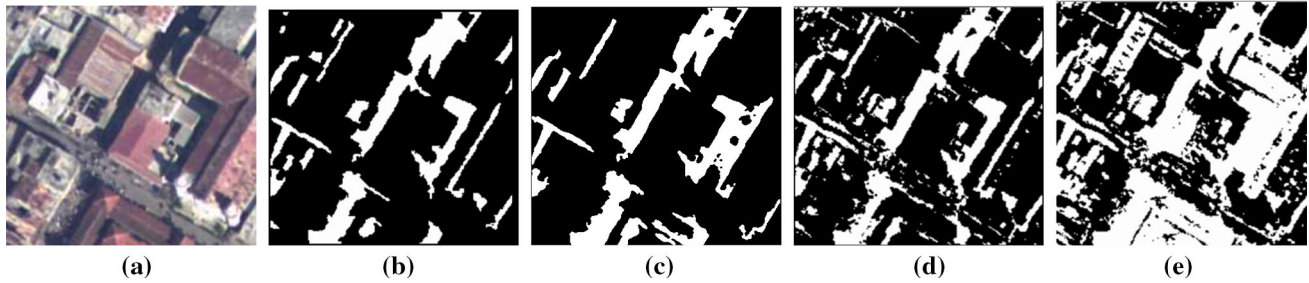


Fig. 7 a–e Show the original image, ground truth image and the output of applying SMS, M4 and M5, on Jacmel Study Area, respectively

Table 7 Performance assessment metrics [15]

		Predicted positive	Predicted negative		
Reference positive		TP	FN		
Reference negative		FP	TN		
Producer's accuracies		User's accuracies		Overall accuracy	F-score
Shadow (recall rate)	Non-shadow	Shadow (precision rate)	Non-shadow		
$P_s = \frac{TP}{TP+FN}$		$P_n = \frac{TN}{TN+FP}$		$U_s = \frac{TP}{TP+FP}$	$U_n = \frac{TN}{TN+FN}$
				$\tau = \frac{TP+TN}{TP+TN+FP+FN}$	$F = 2 \cdot \frac{P_s U_s}{P_s + U_s}$

Table 8 Accuracy assessment of SMS and the five benchmarked algorithms on NOAA aerial image

Method	PA		UA		OA	MCC
	P_s	P_n	U_s	U_n		
SMS	74.76	97.48	90.19	92.60	93.12	0.79
M4	93.33	91.69	72.70	98.30	92.00	0.77
M5	97.98	64.69	39.69	99.26	71.01	0.49

The extension to the multi-thresholding problem using M thresholds is straightforward. For example, in the case of 2-thresholding ($M = 2$), we assume two thresholds with values K_1 and K_2 for separating three classes, C_0 for $[1, \dots, K_1]$, C_1 for $[K_1 + 1, \dots, K_2]$ and C_2 for $[K_2 + 1, \dots, L]$.

The criterion measure or σ_B^2 is then a function of two variables K_1 and K_2 . An optimal set of thresholds K_1^* and K_2^* is selected by maximizing:

$$\sigma_B^2(K_1^*, K_2^*) = \max[\sigma_B^2(K_1, K_2)] \quad (12)$$

3.2 Parameter fine tuning

In the previous subsection, we discussed the theoretical concept behind multi-thresholding segmentation. In real case software implementation, M is considered as a very important parameter that should be defined to determine the number of thresholds used.

As multi-thresholding segmentation depends on the luminance property of the existing objects, we suggest, in this

work, that the value of the number of thresholds M should be set equal to the number of the different surfaces/classes that exist within the studied aerial image. For small values of M such as 1 and 2, background pixels will be incorrectly classified as shadow pixels. This is because when M is small, SMS will work with few luminance surfaces, and therefore, it will be difficult to segment shadow regions correctly.

On the other hand, as M largely increases beyond 6, the shadow of a particular object is segmented into more than one classes. For example, choosing $M = 4$, i.e., roads or background, non-tile flat rooftop buildings, roof tile buildings and shadow objects, the resultant output of detected shadows will be highly compatible with the real shadows contained within the input image. In our future work, we plan to devise an adaptive mechanism to help the users seeking optimality in choosing the value of M . For the rest of this manuscript, we will use $M = 4$ for our experimental scenarios.

In the final results, after applying multi-thresholding segmentation, the first class C_0 corresponds to the building shadows' candidates. However, it might contain some non-shadow objects, and thus, we apply morphological operations, especially the erosion operation with specific structuring elements that fit the non-shadow regions. As the final step, we will use the area condition to validate the presence of building shadows. Shadow area is defined as the number of pixels in the shadow region. This condition is either defined by the user or autonomously computed based on the average area of the potential shadows' candidates. Hence, the SMS approach will detect building shadows and validate them. Future work would include the integration of other criteria such as geometric patterns.

4 Result analysis

In this section, we will benchmark the performance of SMS using two existing reference datasets from the literature: (i) The Toulouse and Norrkoping dataset made of five study areas [15] and (ii) The Jacmel and Strasbourg dataset containing two study areas [22].

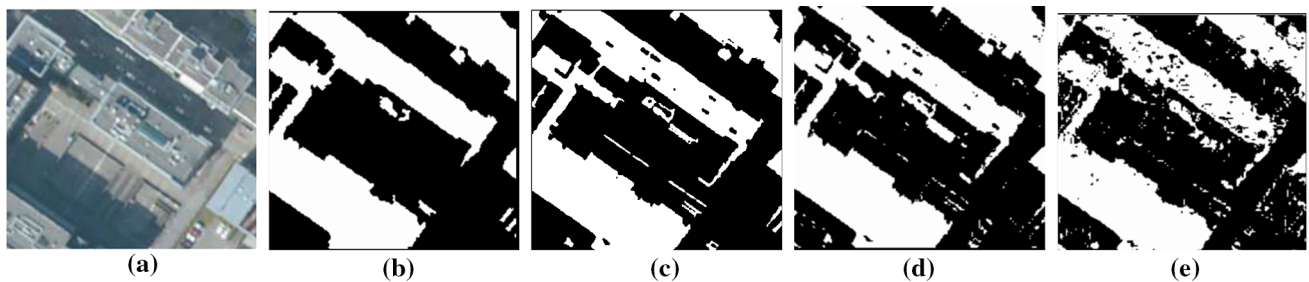


Fig. 8 a–e show the original image, ground truth and the output of applying SMS, M4 and M5, on Strasbourg Study Area, respectively

Table 9 Accuracy assessment of *SMS* and the five benchmarked algorithms on BD ORTHO aerial image

Method	PA		UA		OA	MCC
	P_s	P_n	U_s	U_n		
SMS	88.45	98.00	97.53	80.44	96.21	0.95
M4	93.80	95.48	93.81	95.47	94.77	0.89
M5	88.69	94.38	92.02	91.96	91.98	0.83

4.1 Toulouse and Norrkoping dataset

The authors of [15] categorize the state-of-the-art shadow detection methods into six classes and compare their performance over this specific dataset. Since *SMS* is a threshold-based approach, we will compare its performance with the following threshold-based state-of-the-art algorithms evaluated in [15]: (i) M1: Optimal thresholding on NIR, (ii) M2: First valley detection thresholding on NIR alone and (iii) M3: The modified First valley detection thresholding. More details about these algorithms can be found in [15].

The reference dataset introduced in [15] is an urban dataset with five study areas having high spatial resolution: *Urban Canyon*, *St. Sernin Basilica*, *SubUrban* and *Garonne River* Study Areas shown in Figs. 2a, 3a, 4a and 5a, respectively, are multi-spectral images for Toulouse, France, with a spatial resolution of 0.2 m. The fifth study area, *Industrial*, is located in Norrkoping, Sweden, with a spatial resolution of 0.5 m and is shown in Fig. 6a.

The authors in [15] applied a pixel-based accuracy assessment over the used dataset where new performance metrics were defined. These metrics are summarized in Table 7. The producer's accuracy, *PA*, measures how well the reference pixels are classified in terms of correctness. This is referred to as the over-detection percentage. The user's accuracy metric, *UA*, focuses on the pixels of the classification map that are correct. This is referred to as the under-detection percentage.

The overall accuracy, *OA*, measures the accuracy of the shadow detection algorithms and *F-score* gives a good balance between the under-, and over-detection accuracies. It is also chosen to rank the benchmarked algorithms.

Figure 2 shows the results of applying *SMS* and the benchmarked algorithms over the Urban Canyon Study Area. The accuracy assessment in Table 1 reveals that *SMS* records the highest *F-score* (99.6%) compared to the other three methods *M1*, *M2* and *M3*, which record 95.6%, 95.8% and 97.0%, respectively. The high *PA* coupled with the high *UA* implies that *SMS* resulted in a low *FN* value (low shadows' pixels misclassification).

The results of applying *SMS*, *M1*, *M2* and *M3* over the St. Sernin Basilica Study Area are shown in Fig. 3. We can observe in Table 2 that *SMS* and *M3* have a comparable *F-score* where they outperform the other two methods. *M1* has a high misclassification percentage as the standard Otsu thresholding method did not distinguish between shadows and roads and considered them as one class. This is examined in Fig. 3c.

Figure 4 depicts output results of the Toulouse Suburban Study Area. Table 3 reveals that *SMS* ranks first in terms of *F-score* while *M3* achieves the highest *OA*.

Benchmarked algorithms were also applied to the *Garonne River* Study Area as shown in Fig. 5, and the results are summarized in Table 4. The relatively low U_s compared to the high P_s witnessed for all benchmarked algorithms implies the over-detection of shadows, i.e., some pixels are incorrectly labeled as shadow pixels. This is due to the complex scene environment of the Garonne River. It is interesting to see that *SMS* recorded the highest *F-score* result compared to the other benchmarked methods with a value of 95.1%.

Figure 6 shows the results on the Norrkoping Industrial Study Area. As one can notice in Table 5, *M1* and *M2* do not perform well in terms of *F-score* while *SMS* scores 93.9%.

A closeup of highlighted region (red frame) is shown in Fig. 6f. Interpretation of the results of applying *SMS*, *M1*, *M2* and *M3* algorithms in Figure 6f clearly shows that *SMS* outperforms all other benchmarked algorithms. *M1* mainly did not distinguish between road regions and building shadows, while *M3* falsely classifies some vegetation areas as building shadow. *M2* mis-classifies some shadow pixels as background.

Finally, Table 6 shows the execution time results of applying *SMS* and the three benchmarked algorithms 100 times over each of the five study areas. For this experiment, we used a MacBook Pro machine with a 2.3 GHz Intel Core i7 processor.

The average reported execution time results show that *SMS* ranks first with **0.4925** seconds while *M1* ranks fourth with **1.7197** seconds. In terms of space complexity, *M1* and *M2* are found to be in the order of $O(n)$. The space complexity regarding *SMS*, on the other hand, is in the order of $O(n^2)$ as shown in Table 6.

4.2 Jacmel and Strasbourg dataset

The author in [22] relies on the Jacmel and Strasbourg dataset to present a comprehensive comparison between several shadow detection techniques based on different color and space models. For the scope of this benchmarking technique, we will rely on the following two algorithms investigated in [22]: *M4* which depends on the $C_1C_2C_3$ color space [7] and *M5* which is based on YIQ color space [11].

The Jacmel and Strasbourg dataset consists of the following two study areas: The *Jacmel* Study Area which is a 3-band RGB image with a 24 cm spatial resolution for a part of Jacmel area located in southern Haiti provided by NOAA and shown in Fig. 7a. The *Strasbourg* Study Area made of 3-band RGB image that covers a part of Strasbourg city in northeastern France with a 50 cm spatial resolution and shown in Fig. 8a.

For the accuracy assessment, the author in [22] uses the metrics as defined in Table 7, but instead of adopting the *F-score*, he introduced another metric which is the Matthews Correlation Coefficient (*MCC*). The value of *MCC* as shown in Eq. 13 is bounded between -1 and 1, where larger values indicate a better prediction ratio.

$$MCC = \frac{TP \times TN - FP \times FN}{\sqrt{(TP + FP)(TP + FN)(TN + FP)(TN + FN)}} \quad (13)$$

Figure 7 and Table 8 show the benchmarked algorithms' shadow masks and the accuracy assessment results for the *Jacmel* Study Area. *SMS* outperforms *M4* and *M5* by recording the highest *MCC* value, 0.79.

The accuracy assessment results for the Strasbourg Study Area are presented in Fig. 8 and Table 9. *SMS* also scores the highest *MCC* with a value of 0.95.

5 Conclusion

In this paper, shadow detection of buildings using aerial and high-resolution satellite images is addressed. First, we

have proposed a shadow detection algorithm based on a multi-thresholding segmentation technique that we refer to as *SMS*. Furthermore, *SMS* has been benchmarked against several algorithms over two different reference datasets comprised of seven study areas. Results reveal the exceptional performance of *SMS* in terms of accuracy of shadow detection and computing time.

Funding This study has been funded with support from the National Council for Scientific Research in Lebanon.

Compliance with ethical standards

Conflict of interest The authors declare that they have no conflict of interest.

References

1. Tsai, V.J.D.: A comparative study on shadow compensation of color aerial images in invariant color models. *IEEE Trans. Geosci. Remote Sens.* **44**(6), 1661–1671 (2006)
2. Sirmacek, B., Unsalan, C.: Building detection from aerial images using invariant color features and shadow information. Presented at the 2008 Computer and Information Sciences, 23rd International Symposium, Istanbul, Turkey, 27–29 Oct 2008
3. Massalabi, A., He, D.C., Benie, G.B., Beaudry, E.: Detecting information under and from shadow in panchromatic Ikonos images of the city of Sherbrookel. Presented at the 2004 IEEE International Geoscience and Remote Sensing Symposium (IGARSS), Anchorage, USA, 20–24 Sept 2004
4. Guler, M.A.: Detection of earthquake damaged buildings from post event photographs using perceptual grouping. Master Thesis, Middle East Technical University, Turkey (2004)
5. Seref, A.: Shadow detection and compenation in aerial images with an application to building heigh estimation. Master Thesis, Middle East Technical University, Turkey (2010)
6. Ma, H., Qin, Q., Shen, X.: Shadow segmentation and compensation in high resolution satellite images IEEE international geoscience and remote sensing symposium. Presented at the 2008 IEEE International Geoscience and Remote Sensing Symposium (IGARSS), Boston, USA, 6–11 July 2008
7. Salvador, E., Cavallaro, A., Ebrahimi, T.: Shadow identification and classification using invariant color models. Presented at the 2001 IEEE International Conference on Acoustics, Speech, and Signal Processing. Proceedings (ICASSP), Salt Lake City, USA, 7–11 May 2001
8. Salvador, E., Cavallaro, A., Ebrahimi, T.: Cast shadow segmentation using invariant color features. *Comput. Vis. Image Underst.* **95**(2), 238–259 (2004)
9. Madhavan, B.B., Kikuo, T., Sasagawa, T., Okada, H., Shimozuma, Y.: Automatic extraction of shadow regions in high-resolution ADS40 images by robust approach of feature spaces analysis. In: Proc. ISPRS Congress Istanbul., vol. 35. no. III (2004)
10. Dare, P.M.: A comparative study on shadow compensation of color aerial images in invariant color models. *Photogramm. Eng. Remote Sens.* **71**, 169–177 (2005)
11. Polidorio, A.M., Flores, F.C., Imai, N.N., Tommaselli, A.M.G., Franco, C.: Automatic shadow segmentation in aerial color images. Presented at the 2003 XVI Brazilian Symposium on Computer

- Graphics and Image Processing (SIBGRAPI), Sao Carlos, Brazil, 12–15 Oct 2003
12. Zhang, H., Wenzhuo, L.: Object-oriented shadow detection from urban high-resolution remote sensing images. Presented at the 2014 IEEE Transactions on Geoscience and Remote Sensing, Nov 2014
 13. Zhang, Y., Nan, S., Tian, S.: Shadow detection and removal for occluded object information recovery in urban high-resolution panchromatic satellite images. *IEEE J. Sel. Top. Appl. Earth Obs. Remote Sens.* **9**(6), 2568–2582 (2016)
 14. Khan, S.H., Bennamoun, M., Sohel, F., Togneri, R.: Automatic shadow detection and removal from a single image. *IEEE Trans. Pattern Anal. Mach. Intell.* **38**(3), 431–446 (2016)
 15. Adeline, K.R.M., Chen, M., Briottet, X.: Shadow detection in very high spatial resolution aerial images: a comparative study. *ISPRS J. Photogramm. Remote Sens.* **80**, 21–38 (2013)
 16. Tsai, V.J.D.: Shadow analysis in high-resolution satellite imagery of urban areas. Presented at the 2006 IEEE International Geoscience and Remote Sensing Symposium (IGARSS), Denver, USA, 1–4 Aug 2006
 17. Otsu, N.: A threshold selection method from gray level histograms. *IEEE Trans. Syst. Man Cybern.* **9**(1), 62–66 (1979)
 18. van den Bergh, F., Maharaj, : Adaptive threshold-based shadow masking for across-date settlement classification of panchromatic QuickBird images. *IEEE Geosci. Remote Sens. Lett.* **11**(6), 1153–1157 (2014)
 19. Huang, J., Xie, W., Tang, L.: Detection of and compensation for shadows in colored urban aerial images. Presented at the 2004 5th World Congress on Intelligent Control and Automation, Hangzhou, China, 15–19 June 2004
 20. Wu, T.P., Tang, C.K.: A Bayesian approach for shadow extraction from a single image. Presented at the 2005 IEEE International Conference on Computer Vision (ICCV), Beijing, China, 17–20 Oct 2005
 21. Lin, C., Nevatia, R.: Building detection and description from a single intensity image. *Comput. Vis. Image Underst.* **72**(2), 101–121 (1998)
 22. NGO, T.: Shadow/vegetation and building detection from single optical remote sensing image. Ph.D. Thesis, University of Strasbourg, France (2015)